

High dn_o/dT Liquid Crystals and their Applications in a Thermally Tunable Liquid Crystal Photonic Crystal Fiber

Jun Li

Sebastian Gauza

Shin-Tson Wu

College of Optics and Photonics, University of Central Florida,
Orlando, Florida, USA

Thomas Tanggaard Alkeskjold

Jesper Lægsgaard

Anders Bjarklev

COM Center, Technical University of Denmark, Lyngby, Denmark

We have analyzed the physical origins of the temperature gradient of the ordinary refractive index (dn_o/dT) of liquid crystals. To achieve a large dn_o/dT , high birefringence (Δn) and low clearing temperature play crucial roles. Based on these guidelines, we formulated two exemplary liquid crystal mixtures, designated as UCF-1 and UCF-2. The dn_o/dT of UCF-1 is $\sim 4\times$ higher than that of 5CB at room temperature. By infiltrating UCF-1 into the air holes of a three-rod core photonic crystal fiber, we demonstrate a thermally tunable photonic bandgap fiber with tuning sensitivity of $27\text{ nm}/^\circ\text{C}$ at room temperature. The insertion loss is less than 0.5 dB .

Keywords: high dn_o/dT ; liquid crystals; microstructure devices; photonic crystal fiber

I. INTRODUCTION

Liquid crystals (LCs) have been widely used in display industry, e.g., laptop computers, desktop monitors, projection displays, high-definition TVs, personal digital assistants (PDAs), liquid-crystal-on-silicon (LCoS) for rear projection TVs, etc. [1–4]. Besides displays, LCs are also useful for photonic devices such as optical phased array for laser beam steering [5], light switches [6], variable optical

Address correspondence to Jun Li, College of Optics and Photonics, University of Central Florida, Orlando, 32816 Florida, USA. E-mail: swu@mail.ucf.edu

attenuator [7], thermal solitons in nematic LCs [8,9], and thermally tunable LC photonic crystal fibers [10–12]. For laser beam steering, high birefringence (Δn) and low viscosity LCs are preferred in order to obtain fast response time. On the other hand, LC materials with a high temperature gradient in refractive indices, especially the ordinary refractive index, are highly desirable for triggering the thermal solutions in nematic liquid crystals and for improving the thermal tuning sensitivity of the bandgaps of a liquid crystal photonic crystal fiber (LCPCF).

Comparing with isotropic liquids, LCs have inherent large temperature gradients for both n_e (extraordinary ray) and n_o (ordinary ray). For some commercial LC compounds such as 5CB and 6CB, their temperature gradient of the refractive indices is $\sim 10^{-4}$ at room temperature (RT). A small dn_o/dT means that a higher laser power is needed in order to observe the thermal effect. To enhance the dn_o/dT value, new LC mixtures need to be developed [13].

In this paper, we analyze the factors affecting the dn_o/dT of a LC material based on the four-parameter model, which describes the temperature-dependent refractive indices. Guidelines are developed for tailoring new LC materials with high dn_o/dT at RT. Two new LC mixtures, designated as UCF-1 and UCF-2 are formulated in our lab. A highly tunable large-core single-mode photonic bandgap fiber was infiltrated with UCF-1 into the micro holes around the silica core of a three-rod core photonic crystal fiber. A bandgap tuning sensitivity of 27 nm/°C is achieved at RT. The insertion loss is estimated to be less than 0.5 dB and mainly caused by coupling loss between the index-guided mode and the bandgap-guided mode. In Sec. II, we derived the physical models for dn_o/dT , temperature gradient of ordinary refractive index, and dn_e/dT , temperature gradient of extraordinary refractive index based on the four-parameter model. The factors affecting dn_o/dT are disclosed. In Sec. III, we describe the compositions of UCF-1 and UCF-2 which have a large dn_o/dT at RT. The electro-optic properties of these two mixtures are presented. We also compare the dn_o/dT value of these two new mixtures with 5CB and 6CB. In Sec. IV, we evaluate the highly tunable LC photonic crystal fiber by infiltrating UCF-1 into a section of three-rod core photonic crystal fiber with 10 mm length.

II. THEORY

Based on the Vuks model [14] and Haller equation [15], we derived the four-parameter model for describing the temperature effect on LC refractive indices. Equations (1a) and (1b) show the expressions for

the four-parameter model [16]:

$$n_e(T) = A - BT + \frac{2(\Delta n)_o}{3} \left(1 - \frac{T}{T_c}\right)^\beta, \quad (1a)$$

$$n_o(T) = A - BT - \frac{(\Delta n)_o}{3} \left(1 - \frac{T}{T_c}\right)^\beta. \quad (1b)$$

Although Eq. (1) has four parameters, they are obtained by pairs: A and B are obtained by fitting the temperature dependent average refractive index $\langle n \rangle$ using Eq. (2), while $(\Delta n)_o$ and β are obtained by fitting the birefringence Δn using the Haller equation which is shown in Eq. (3) [13,16]:

$$\langle n(T) \rangle = A - BT \quad (2)$$

$$\Delta n(T) = (\Delta n)_o \left(1 - \frac{T}{T_c}\right)^\beta \quad (3)$$

Equation (2) indicates that the average refractive index of LCs decreases linearly as temperature increases in the nematic range. In Eq. (3), $(\Delta n)_o$ is the birefringence in the crystalline state and β is a material constant which is not too sensitive to the LC structures.

Taking the temperature derivatives of Eq. (1), we derive the following equations to describe the temperature gradient of LC refractive indices [13,17]:

$$\frac{dn_e}{dT} = -B - \frac{2\beta(\Delta n)_o}{3T_c \left(1 - \frac{T}{T_c}\right)^{1-\beta}}, \quad (4a)$$

$$\frac{dn_o}{dT} = -B + \frac{\beta(\Delta n)_o}{3T_c \left(1 - \frac{T}{T_c}\right)^{1-\beta}}. \quad (4b)$$

In Eq. (4a), both terms in the right-hand side are negative, independent of the temperature. This implies that n_e decreases as the temperature increases throughout the entire nematic range. However, Eq. (4b) consists of a negative term ($-B$) and a positive term which depends on the temperature. In the low temperature regime ($T \ll T_c$), the positive term could be smaller than the absolute value of the negative term resulting in a negative dn_o/dT . As the temperature increases, the positive term also increases. As T approaches T_c , dn_o/dT jumps to a large positive number. In the intermediate, there exists a transition temperature at which $dn_o/dT = 0$. We define this temperature as the

crossover temperature T_o for n_o . To find T_o , we simply solve $dn_o/dT = 0$ from Eq. (4b). In the $T < T_o$ regime, n_o decreases as temperature increases, but when $T > T_o$, n_o increases as temperature increases. Beyond the clearing point T_c , n_o equals to n_e and the optical anisotropy disappears [13].

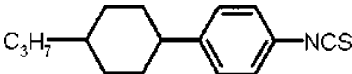
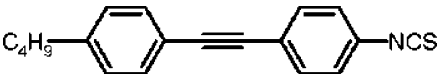
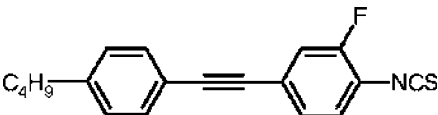
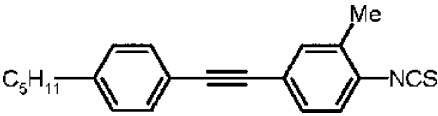
From Eq. (4b), dn_o/dT is determined by five parameters (B , β , $(\Delta n)_o$, T and T_c). Among these five, β and T can be treated as constants: $\beta \sim 0.2$ and $T \sim 295$ K since the preferred operation temperature is around RT. Therefore, we only need to consider the remaining three parameters: B , $(\Delta n)_o$, and T_c . A smaller B helps to boost the dn_o/dT value. Among the LC materials investigated, we found that the compounds containing isothiocyanato (NCS) polar group possess a slightly smaller B coefficient and higher birefringence than the cyano (CN) compounds. Some experimental evidences will be shown later. Therefore, the remaining two parameters, high birefringence and low clearing temperature, play crucial roles in determining the dn_o/dT and crossover temperature. However, these two requirements are often contradicting to each other. Most of the high birefringence LC compounds are associated with high melting and clearing temperatures due to their long molecular conjugation. From Eq. (4b), the T_c effect is particularly significant. If the T_c of a LC material is much higher than room temperature, then its crossover temperature would be relatively high and $dn_o/dT < 0$ at RT. Mixture E7 is such an example; its T_c is $\sim 60^\circ\text{C}$ and its dn_o/dT is negative at RT. That is why the n_o of E7 decreases as temperature increases in the low temperature range.

Although a large positive dn_o/dT can always be obtained by raising the operating temperature toward the clearing point, in practice this is undesirable for two reasons. First, in this regime a small temperature fluctuation would cause a large dn_o/dT change. Second, light scattering due to LC director fluctuations is strong near the phase transition [18]. Many devices are preferred to operate at room temperature. Thus, it is highly desirable to design a LC mixture exhibiting a large dn_o/dT at room temperature.

III. NEW LC MIXTURES

To design mixtures with high birefringence and low clearing temperature, we selected some laterally substituted isothiocyanato tolanes [19]. Due to the lateral fluoro or methyl substitution, these NCS tolanes exhibit a relatively low clearing temperature. The molecular structures and their corresponding phase transition temperatures (PTT) are listed in Table 1.

TABLE 1 Molecular Structures and Phase Transition Temperatures (PTT) of the Compounds used for Formulating Mixtures. Here, Cr, N, S, and I Stand for Crystalline, Nematic, Smectic, and Isotropic Phase, Respectively

LC compounds	Structures	PTT (°C)
CP3NCS		Cr 39.0 N 41.3 I
PTP4NCS		Cr 44.0 S _K 70.5 S _E 86.9 I
PTP(3F)4NCS		Cr 38.6 I
PTP(3Me)5NCS		Cr 42.3 I

The phase transition temperatures of these LC compounds were measured by using a high sensitivity differential scanning calorimeter (DSC, TA Instrument Model Q-100) at 2°C/min scanning rate. By changing the ratio of these single compounds, we prepared two mixtures, designated as UCF-1 and UCF-2. Their clearing temperatures are 29.7°C and 32.3°C, respectively, and melting point below -20°C. The physical properties of UCF-1 and UCF-2 were measured at RT ~23°C. Results are listed in Table 2.

We measured the refractive indices of our new mixtures and compared results with three commercial single compounds: 5CB, 6CB, and 5PCH (cyano-cyclohexane-phenyl). These LCs are nematic at room temperature and have been used in many LC mixtures. To

TABLE 2 Physical Properties of UCF-1 and UCF-2. Δn was Measured at $\lambda = 589$ nm and $T = 23^\circ\text{C}$

LC materials	$V_{th}(V_{rms})$	$\epsilon_{ }$	ϵ_{\perp}	$\Delta\epsilon$	$K_{11}(\text{pN})$	$K_{33}(\text{pN})$	Δn
UCF-1	1.01	13.6	5.2	8.4	4.66	11.4	0.2545
UCF-2	1.15	13.6	4.9	8.7	5.90	11.0	0.2755

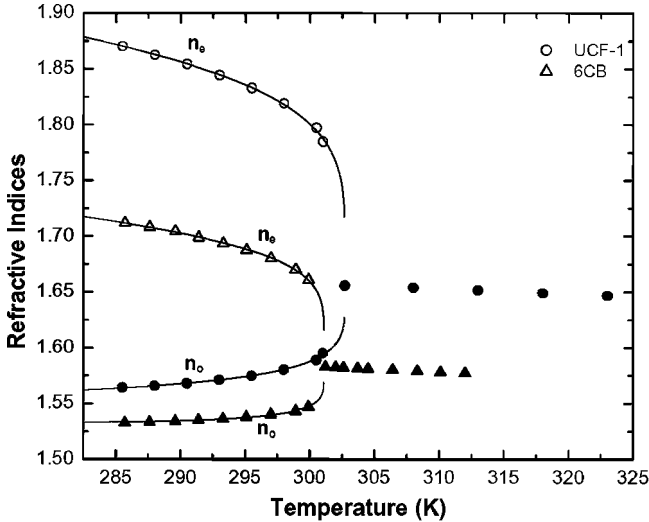


FIGURE 1 Temperature-dependent refractive indices of UCF-1 and 6CB at $\lambda = 589$ nm. Circles and triangles are refractive indices of UCF-1 and 6CB, respectively. Solid lines are fittings using Eqs. (1a) and (1b). The fitting parameters are listed in Table 3.

measure refractive indices, we use a multi-wavelength Abbe refractometer (Atago DR-M4) which can be used to measure the LC refractive indices at $\lambda = 450, 486, 546, 589, 633,$ and 656 nm. The accuracy of the Abbe refractometer is up to the fourth decimal. For a given wavelength, we measured the refractive indices of 5CB, 6CB, UCF-1, and UCF-2 from 10 to 60°C , respectively. The temperature of the Abbe refractometer is controlled by a circulating constant temperature bath (Atago Model 60-C3). The LC molecules are aligned perpendicular to the main prism surface of the Abbe refractometer by coating a surfactant comprising of 0.294 wt.% hexadecyltri-methyl-ammonium bromide in methanol solution. Both n_e and n_o are obtained through a polarizing eyepiece.

To demonstrate the high Δn advantage, we intentionally designed the UCF-1 and UCF-2 to have similar clearing temperatures as 6CB and 5CB, respectively. Figure 1 depicts the temperature dependent refractive indices of UCF-1 and 6CB at $\lambda = 589$ nm. Circles and triangles represent experimental data for UCF-1 and 6CB, respectively, while solid lines are the fitting results using Eqs. (1a) and (1b). The fitting parameters $[A, B]$ and $[(\Delta n)_0, \beta]$ are listed in Table 3. The agreement between experiment and theory is pretty good. In Figure 1, UCF-1 has a higher n_e , n_o , and Δn than 6CB. At room temperature

TABLE 3 Fitting Parameters for the Average Refractive Index $\langle n \rangle$ and Birefringence (Δn) of the Five LCs Studied: UCF-1, 6CB, UCF-2, 5CB and 5PCH at $\lambda = 589$ nm

LC materials	$\langle n \rangle$		Δn	
	A	B (K^{-1})	$(\Delta n)_o$	β
UCF-1	1.8112	5.08×10^{-4}	0.5397	0.1973
6CB	1.7491	5.47×10^{-4}	0.3026	0.1780
UCF-2	1.8100	4.90×10^{-4}	0.5416	0.1936
5CB	1.7674	5.79×10^{-4}	0.3505	0.1889
5PCH	1.6795	5.07×10^{-4}	0.1705	0.1512

($T \sim 295$ K), the birefringence of UCF-1 is $\Delta n \sim 0.25$, as compared to ~ 0.15 for 6CB. As temperature increases, n_e decreases while n_o increases for both UCF-1 and 6CB except at a different rate. The clearing point for UCF-1 and 6CB is 302.7 K and 301.1 K, respectively. In the isotropic state, the refractive index of UCF-1 and 6CB decreases linearly with increasing temperature. From Figure 1, we find UCF-1 has a much larger dn_o/dT than 6CB in the nematic range. We will compare the dn_o/dT quantitatively for all the LCs studied later [13].

Similarly, we prepared UCF-2 to match the clearing temperature of 5CB. The clearing point for UCF-2 and 5CB is 305.3 K and 306.4 K, respectively. Figure 2 depicts the temperature dependent refractive indices of UCF-2 and 5CB at $\lambda = 589$ nm. Circles and triangles represent experimental data for UCF-2 and 5CB, respectively, while solid lines are fitting results using Eqs. (1a) and (1b). The fitting parameters A , B , $(\Delta n)_o$ and β are also listed in Table 3. From Figure 2, UCF-2 has a higher n_e , n_o , and Δn than 5CB.

Using the parameters listed in Table III, we are able to calculate the dn_e/dT and dn_o/dT for UCF-1, UCF-2, 6CB, 5CB, and 5PCH using Equation (4). Because dn_e/dT is always negative, we plot $-dn_e/dT$ instead. Results are shown in Figure 3 where solid and dashed lines represent the calculated dn_o/dT and $-dn_e/dT$ by using Eq. (4) for these five LCs, respectively. From Figure 3, we find the dn_e/dT (dashed lines) for both LCs remains negative throughout their nematic range. That means the extraordinary refractive index decreases as the temperature increases in the entire nematic range. However, dn_o/dT changes sign at the crossover temperature T_o . For practical applications, it is desirable to operate the LC device at room temperature (RT). Therefore, we should design a LC with crossover temperature lower than 295 K to assure a positive dn_o/dT at RT. From Figure 3, the crossover temperature (T_o) of UCF-1, UCF-2, 6CB, 5CB, and

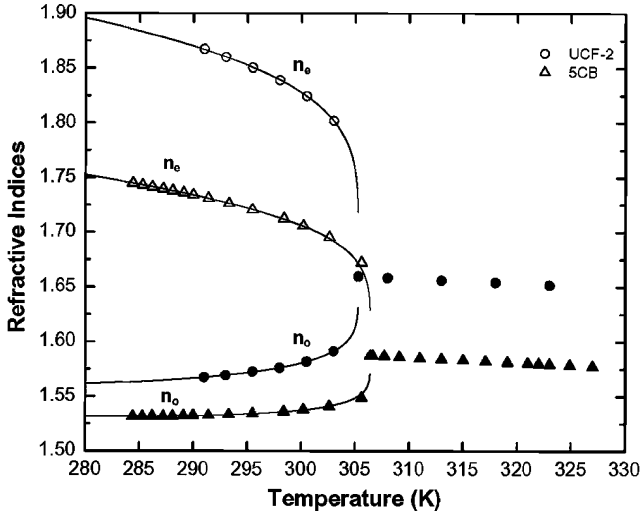


FIGURE 2 Temperature-dependent refractive indices of UCF-2 and 5CB at $\lambda = 589$ nm. Circles and triangles are refractive indices of UCF-2 and 5CB, respectively, and solid lines are fitting results using Eqs. (1a) and (1b). The fitting parameters are listed in Table 3.

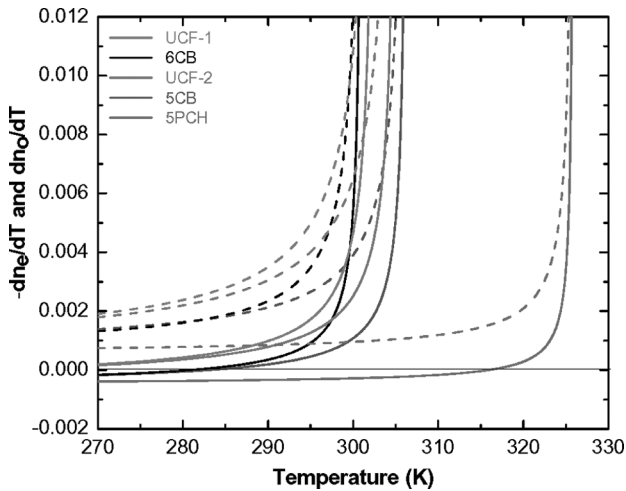


FIGURE 3 Temperature-dependent dn_o/dT of UCF-1, UCF-2, 6CB, 5CB, and 5PCH at $\lambda = 589$ nm. Solid lines represent the calculated dn_o/dT curves for UCF-1, UCF-2, 6CB, 5CB, and 5PCH, respectively, while the dashed lines represent the calculated $-dn_e/dT$ curves. The parameters B , $(\Delta n)_o$, and β used in the calculations are listed in Table 3.

5PCH is ~ 254 K (or -19°C), ~ 255 K (or -18°C), ~ 280.8 K (or 7.8°C), ~ 282.9 K (or 9.9°C) and ~ 315.9 K (or 42.9°C), respectively. Based on Eq. (4b), low T_c and high birefringence are two important factors for achieving a large dn_o/dT at RT. The clearing point for UCF-1, UCF-2, 6CB, 5CB and 5PCH is 302.7 K, 305.3 K, 301.1 K, 306.4 K, and 326 K, respectively. Thus, the n_o of UCF-1, UCF-2, 6CB, and 5CB increases with increasing temperature when T is greater than RT but less than T_c . For 5PCH, its crossover temperature is higher than RT so that its dn_o/dT remains negative when $T < T_o$. The crossover temperature we obtained for 5PCH agrees very well with the experimental data reported by the Merck group [20]. As the temperature approaches T_c , both dn_e/dT and dn_o/dT change dramatically as shown clearly in Figure 3.

The large dn_o/dT helps improve the thermally tuning sensitivity of the positions of the bandgaps of the liquid crystal photonic crystal fiber (LCPCF) and lower the required laser power for triggering the thermal soliton in nematic liquid crystal. From Figure 3, the dn_o/dT (in unit of K^{-1}) of UCF-1, UCF-2, 6CB, and 5CB at RT is 1.73×10^{-3} , 1.27×10^{-3} , 9.24×10^{-4} , and 4.60×10^{-4} , respectively. Due to the higher birefringence and a slightly lower clearing temperature, the dn_o/dT of UCF-1 is $\sim 4\times$ higher than that of 5CB at RT. As T approaches T_c , the dn_o/dT of each LC increases by more than one order of magnitude than that in the nematic phase. However, in the vicinity of phase transition temperature, a small temperature fluctuation would cause a big change in dn_o/dT . Moreover, light scattering is present as the temperature is near the phase transition. In the following section, we show the application of these new mixtures in a thermally tunable liquid crystal photonic crystal fiber.

IV. LIQUID CRYSTAL PHOTONIC CRYSTAL FIBER

Photonic crystal fibers (PCFs), also referred to as microstructured optical fibers, have a microstructured cross-section of air holes running along the length of the fiber, which is usually made from silica. For certain applications, it is desirable to dynamically alter the transmission properties of the fiber and, thereby, tune/trim them. For example, in applications involving dispersion, polarization or attenuation, the transmission properties can be changed while keeping the signal within the fiber. For this purpose, photonic crystal fibers are an interesting candidate, since the air holes give close access to the guided light in the core and opens up for using liquids or liquid crystals infiltrated into the capillaries instead of air [10,21]. The optical properties of the liquids or liquid crystals are usually easier to modify

than the silica, and this, therefore, opens up a new application for the tunable PCF-based components.

The photonic bandgaps of a LC-filled PCF can be thermally tuned using nematic, smectic A, and cholesteric mesophases, and these phases yield different functionalities such as threshold switching or linear shifting of the bandgaps. In this case, it is desirable to have a high tuning sensitivity around room temperature in order to decrease the power consumption and ease the device handling. The tuning sensitivity of the spectral positions of the bandgaps is directly related to the temperature gradient of the ordinary refractive index of the infiltrated LC. High and positive temperature gradient of the ordinary refractive index at room temperature produces a high thermal tuning sensitivity for LCPCFs with planar aligned nematics. Further, for applications involving for example dispersion trimming of short laser pulses with high peak power it is desirable to use single-mode PCFs having a very large mode area in order to have a small fraction of the field propagating in the LC. We have demonstrated a highly tunable large-core single-mode photonic bandgap fiber, which has a core diameter of $25\ \mu\text{m}$, an effective mode area of $440\ \mu\text{m}^2$ and a high tuning sensitivity near room temperature [13]. This is achieved using UCF-1 and a three-rod core PCF [22].

In this experiment we used two meters of a so-called LMA25 PCF, where the core is surrounded by six rings of air holes arranged in a triangular lattice (Fig. 4). The hole diameter (d), inter hole distance (Λ), core size and outer diameter was $2.9\ \mu\text{m}$, $11.2\ \mu\text{m}$, $25\ \mu\text{m}$ and $470\ \mu\text{m}$, respectively. The large mode-area is obtained using a three-rod core design. The endlessly single mode property for index-guiding is retained by scaling the relative hole diameter to $d/\Lambda = 0.26$, which is slightly larger than the theoretical limit of 0.25. High leakage and bend loss was observed for $\lambda < 1\ \mu\text{m}$ due to the relatively small air holes.

First, the air holes were filled with E7 nematic LC mixture (Merck) for 10 mm long using capillary forces. The LC was heated to isotropic phase and cooled down again slowly to achieve a homogenous alignment. Polarized optical microscopy observations on a single silica capillary tube, with $6\ \mu\text{m}$ inner diameter, indicate that the LC was planar aligned, i.e., with the LC director aligned along the fiber axis. Therefore, the ordinary index (n_o) predominantly determines the spectral features of the fiber. Figure 4 shows the transmission spectrum at temperatures between $T = 40^\circ\text{C}$ and 55°C in steps of 5°C . The transmission spectrum was obtained by butt-coupling an endlessly single mode PCF with $10\ \mu\text{m}$ core diameter to both ends of the LMA25. The light from a halogen-tungsten white light source was coupled into one end and the transmission spectrum was recorded by an optical

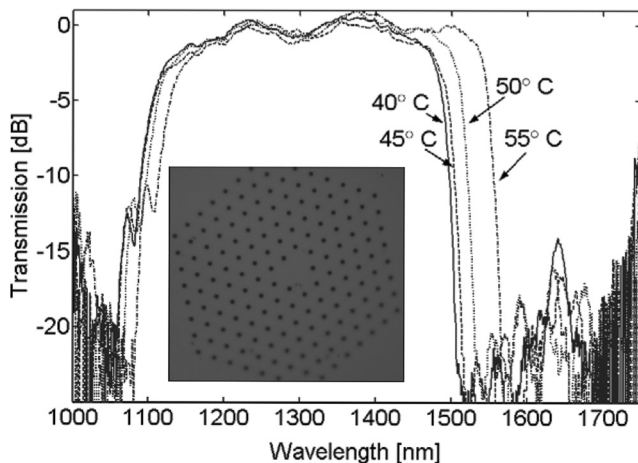


FIGURE 4 Transmission spectrum for the three-rod core PCF. The air holes are filled for 10 mm long with E7. Inset shows an optical micrograph of the PCF end facet. Hole diameter and inter hole distance is $2.9\ \mu\text{m}$ and $11.2\ \mu\text{m}$, respectively.

spectrum analyser (ANDO AQ6317B) and normalized to the spectrum of an un-filled fiber.

From Figure 4, the bandgap centered at $\lambda \sim 1300\ \text{nm}$ has a bandwidth of 345–410 nm, which depends on the temperature. As the temperature increases, the central wavelength of the bandgap shifts toward longer wavelength due to a positive dn_o/dT , which increases as the clearing temperature of E7 is approached. At the same time, the bandwidth of the bandgap increases, which implies that the shorter and longer bandgap edges to experience a different shift; the long wavelength edge experiences a larger shift than the short wavelength edge. The tuning sensitivity at 52.5°C was measured at the long wavelength edge of the bandgap to $7\ \text{nm}/^\circ\text{C}$ or 0.46% per $^\circ\text{C}$ when normalized to the central wavelength at the bandgap edge. The small transmission peak at $1650\ \text{nm}$ is a direct feature of the LC anisotropy, which causes a splitting in effective index of the TE_{01} and the TM_{01} cladding states supported by a LC infiltrated micro channel. The splitting is observed since the electric field of the TE_{01} is solely in the transversal direction, while the TM_{01} has a part of the electric field in the longitudinal direction. The TM_{01} mode, therefore, experiences the extraordinary index of the LC and a gap in effective index is formed between the bands derived from the TE_{01} and TM_{01} cladding states.

The insertion loss of the LC device is difficult to establish exactly due to Fabry-Perot effects between the two end-facets forming the butt

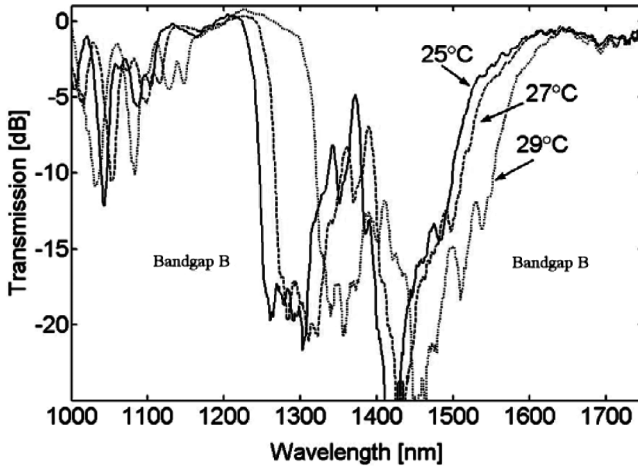


FIGURE 5 Temperature dependent transmission spectra for the three-rod core PCF. The air holes are filled for 10 mm long with UCF-1.

coupling, which cause ripples in the transmission spectrum. We estimate the loss to be less than 0.5 dB.

The tuning sensitivity at room temperature can be increased using an optimized LC mixture, which has a high dn_o/dT at room temperature. Therefore, another LCPCF sample was prepared using UCF-1. Polarized optical microscopy observations on a single capillary tube with UCF-1 also indicated a planar alignment of the LC director. Figure 5 shows the transmission spectrum for the filled PCF. The spectrum shows high transmission in two bandgaps, bandgap A centered at ~ 1150 nm and bandgap B centered at ~ 1700 nm. In between these two bandgaps, a weaker transmission peak appears. This feature is also a direct consequence of the LC anisotropy, which causes a splitting of the EH_{11} mode of an LC-infiltrated microchannel from the HE_{12} and HE_{31} modes [11,23] so that a narrow bandgap opens up between the cladding states derived from these modes. As observed from Figure 5, the width and transmission of the bandgap is reduced as the temperature of UCF-1 is increased, which is due to a decreasing anisotropy as the temperature approaches the clearing temperature of UCF-1 ($T_c = 29.7^\circ\text{C}$), whereby the splitting of the EH_{11} , HE_{12} , and HE_{31} cladding modes is diminished.

Figure 6 plots the measured refractive indices of UCF-1 and fitted data using the extended Cauchy equations [24,25]. The extrapolated data in the near-infrared spectrum are used to perform simulations [26].

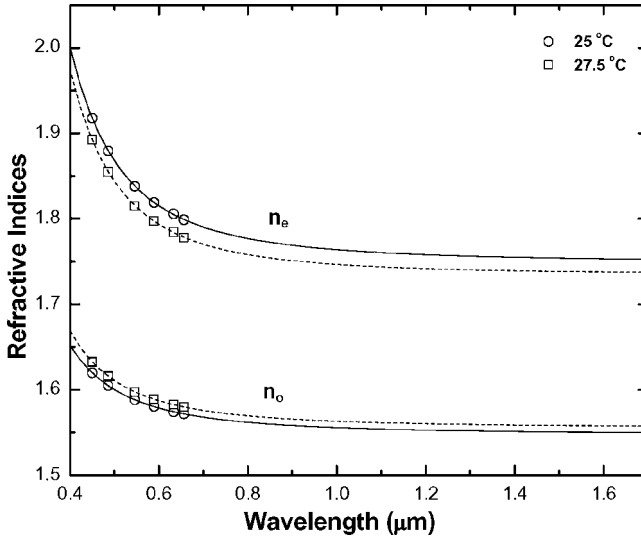


FIGURE 6 Wavelength- and temperature-dependent refractive indices n_e and n_o of UCF-1 at $T = 25^\circ\text{C}$ and 27.5°C . Circles and rectangles are measured refractive indices at $\lambda = 450, 486, 546, 589, 633,$ and 656 nm and at $T = 25^\circ\text{C}$ and 27.5°C , respectively. Solid and dashed lines are fitting curves using the extended Cauchy equation. The fitting curves are extrapolated to the infrared region based on the experimental data measured in the visible spectral region.

Figure 7 compares the measured normalized transmission spectrum of bandgap B and the simulation results of two-times the coupling loss between the index-guided mode (unfilled PCF) and the bandgap-guided mode (LC filled PCF) evaluated using overlap integrals and the refractive indices of UCF-1 shown on Figure 6. Insets show the simulated mode fields of the index-guided mode in an unfilled PCF (TIR mode), a PBG guided mode at the center and at the short wavelength edge of the bandgap. The simulated coupling loss agrees well with the shape of the PBG spectrum, and it is, therefore, concluded that coupling loss ($< 0.5\text{ dB}$) is the dominant loss mechanism, as was also found by Steinvurzel *et al.* [27]. The deviation at $\lambda > 1.65\ \mu\text{m}$ is caused by temporal intensity fluctuations of the halogen-tungsten white light source. The spectral tuning sensitivity of the UCF-1 infiltrated PCF at 28°C was measured at the long wavelength edge of bandgap A to be $27\text{ nm}/^\circ\text{C}$ or 2.1% when normalized. The tuning sensitivity at room temperature using UCF-1 is, therefore, approximately 4.6X higher than when using E7 at above 50°C , which is directly related to the higher temperature gradient of UCF-1 at

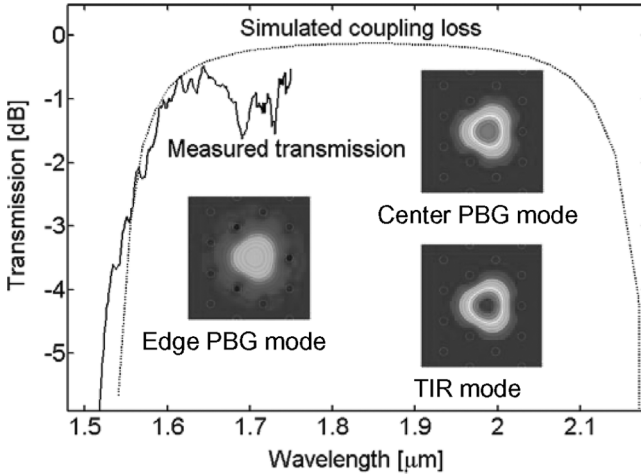


FIGURE 7 Transmission spectrum of the UCF-1 filled PCF (solid line) and simulated coupling loss (dotted line) from the index-guiding to the bandgap-guiding part of the PCF. Insets show an index-guided mode and PBG guided modes at the bandgap center and edge.

room temperature as compared to E7 shown in Figure 8. The temperature gradient at $\lambda = 589$ nm was calculated using a four-parameter model [16] for describing the temperature effect on the LC refractive

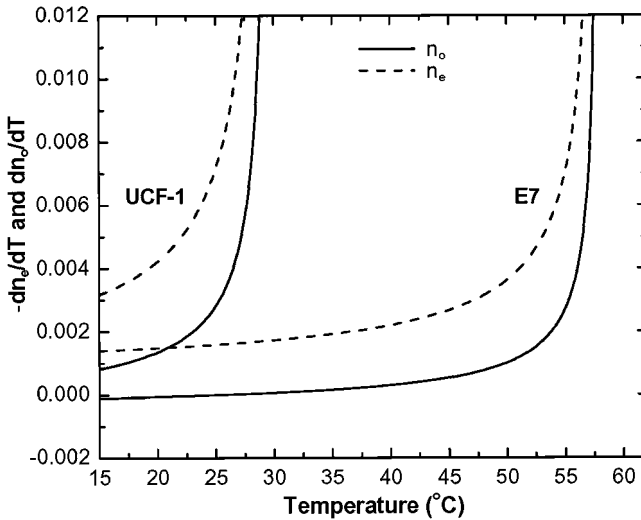


FIGURE 8 dn_o/dT and $-dn_e/dT$ for E7 and UCF-1 calculated at $\lambda = 589$ nm.

indices. The four parameters were obtained by fitting the temperature dependent LC refractive indices measured at temperature from 15 to 55°C with a 5°C interval and at $\lambda = 589$ nm.

V. CONCLUSIONS

We have analyzed the factors affecting the dn_o/dT of a LC material. High birefringence and low clearing temperature are the two most critical parameters. Based on these simple guidelines, we formulated two exemplary high birefringence and low clearing temperature LC mixtures, UCF-1 and UCF-2, using the laterally substituted isothiocyanato tolane compounds. The dn_o/dT of UCF-1 is about 4X higher than that of 5CB at room temperature. Moreover, the melting temperature of UCF-1 and UCF-2 is below -20°C , which is much lower than that of 5CB and 6CB.

The new high dn_o/dT LC mixtures greatly improve the thermal tuning sensitivity of liquid crystal photonic crystal fibers. A highly tunable single mode photonic bandgap fiber device has been demonstrated, which utilizes a three-rod core PCF infiltrated with UCF-1 in order to obtain a large mode area and high tuning sensitivity. The guided mode has an effective area of $440\ \mu\text{m}^2$ with an insertion loss of less than 0.5 dB. The loss is mainly attributed to coupling losses between the index-guided section and the bandgap-guided section. The thermal tuning sensitivity of the spectral position of the bandgap was measured to be $27\ \text{nm}/^\circ\text{C}$ at near room temperature. The tuning sensitivity is $4.6 \times$ higher than that infiltrated with E7, operated at a temperature above 50°C .

REFERENCES

- [1] Wu, S. T. & Yang, D. K. (2001). *Reflective Liquid Crystal Displays*, Wiley: New York.
- [2] Stupp, E. & Brennessoltz, M. (1999). *Projection Display*, Wiley: New York.
- [3] Alt, P. M. (1997). Conference record of the Int'l Display Research Conf. M19-28.
- [4] Fan-Chiang, K. H., Wu, S. T., & Chen, S. H. (2005). *J. Display Technology*, 1, 304.
- [5] McManamon, P. F., Dorschner, T. A., Corkum, D. L., Friedman, L., Hobbs, D. S., Holz, M., Liberman, S., Nguyen, H. Q., Resler, D. P., Sharp, R. C., & Watson, E. A. (1996). *Proc. of the IEEE*, 84, 268.
- [6] Soref, R. A. (1979). *Opt. Lett.*, 4, 155.
- [7] Hirabayashi, K., Wada, M., & Amano, C. (2001). *J. Lighwave Techn.*, 13, 609.
- [8] Warenghem, M., Henninot, J. F., & Abbate, G. (1998). *Opt. Express*, 2, 483.
- [9] Warenghem, M., Henninot, J. F., Derrin, F., & Abbate, G. (2002). *Mol. Cryst. Liq. Cryst.*, 373, 213.
- [10] Larsen, T. T., Bjarklev, A., Hermann, D. S., & Broeng, J. (2003). *Opt. Express*, 11, 2589.
- [11] Alkeskjold, T. T., Lægsgaard, J., Bjarklev, A., Hermann, D. S., Anawati, A., Li, J., & Wu, S. T. (2004). *Opt. Express*, 12, 5857.

- [12] Alkeskjold, T. T., Lægsgaard, J., Bjarklev, A., Hermann, D. S., Broeng, J., Li, J., Gauza, S., & Wu, S. T. (2005). *Applied Optics.*, *45*, 2261.
- [13] Li, J., Gauza, S., & Wu, S. T. (2004). *Opt. Express*, *12*, 2002.
- [14] Vuks, M. F. (1966). *Opt. Spektrosk.*, *20*, 644.
- [15] Haller, I. (1975). *Prog. Solid State Chem.*, *10*, 103.
- [16] Li, J., Gauza, S., & Wu, S. T. (2004). *J. Appl. Phys.*, *96*, 19.
- [17] Li, J., Wen, C. H., Gauza, S., Lu, R., & Wu, S. T. (2005). *J. Display Technology*, *1*, 51.
- [18] Wu, S. T. & Lim, K. C. (1987). *Appl. Opt.*, *26*, 1722.
- [19] Gauza, S., Wang, H., Wen, C. H., Wu, S. T., Seed, A. J., & Dąbrowski, R. (2003). *Jpn. J. Appl. Phys.*, Part 2, *42*, 3463.
- [20] Pohl, L. & Finkenzeller, U. (1990). *Liquid Crystals: Applications and Uses*, World Scientific: Singapore.
- [21] Eggleton, B. J., Kerbage, C., Westbrook, P. S., Windeler, R., & Hale, A. (2001). *Opt. Express*, *9*, 698.
- [22] Mortensen, N. A., Nielsen, M. D., Folkenberg, J. R., Petersson, A., & Simonsen, H. R. (2003). *Opt. Lett.*, *28*, 393.
- [23] Dai, J. D. & Jen, C. K. (1991). *J. Opt. Soc. Am. A*, *8*, 2021.
- [24] Li, J. & Wu, S. T. (2004). *J. Appl. Phys.*, *95*, 896.
- [25] Li, J. & Wu, S. T. (2004). *J. Appl. Phys.*, *96*, 170.
- [26] Li, J., Wu, S. T., Brugioni, S., Faetti, S., & Meucci, R. (2005). *J. Appl. Phys.*, *97*, 073501.
- [27] Steinvurzel, P., Kuhlmeier, B. T., White, T. P., Steel, M. J., de Sterke, C. M., & Eggleton, B. J. (2004). *Opt. Express*, *12*, 5424.